

Projective Quantum Monte Carlo Method for the Anderson Impurity Model and its Application to Dynamical Mean Field Theory

M. Feldbacher,¹ K. Held,¹ and F. F. Assaad²

¹Max-Planck-Institut für Festkörperforschung, Heisenbergstraße 1, D-70569 Stuttgart

²Universität Würzburg, Institut für Theoretische Physik I, Am Hubland, 97074 Würzburg

(Dated: August 24, 2018)

We develop a projective quantum Monte Carlo algorithm of the Hirsch-Fye type for obtaining ground state properties of the Anderson impurity model. This method is employed to solve the self-consistency equations of dynamical mean field theory. It is shown that the approach converges rapidly to the ground state so that reliable zero-temperature results are obtained. As a first application, we study the Mott-Hubbard metal-insulator transition of the one-band Hubbard model, reconfirming the numerical renormalization group results.

In recent years, we have seen a revival of interest in Kondo-like physics, in particular in quantum dot systems [1], adatoms on surfaces [2], and in connection with the dynamical mean field theory (DMFT) [3, 4]. The underlying microscopic model, the Anderson impurity model (AIM), can be solved exactly by Bethe ansatz [5] for the special case of a linear dispersion relation. But in general, such a solution is only possible numerically. Two sophisticated numerical techniques have been established in the literature: the numerical renormalization group (NRG) [6] and the Hirsch-Fye quantum Monte Carlo (HF-QMC) [7] method.

In his pioneering work [6], Wilson applied the renormalization group concept to the Kondo problem: High energy degrees of freedom are systematically integrated out and one obtains an excellent description of the low energy degrees of freedom, which was not possible before since perturbation theory for the AIM breaks down at low temperatures and energies. Confirming earlier scaling ideas of Anderson [8], these NRG calculations show the formation of a low-energy Kondo singlet between the AIM localized and conduction electrons and an associate Abrikosov-Suhl resonance in the spectrum.

The same physics can be described by the HF-QMC algorithm. This method solves the AIM numerically by discretizing the imaginary time interval $[0, \beta]$ ($\beta = 1/T$: inverse temperature) into steps of size $\Delta\tau$ and by mapping the interacting AIM onto a sum of non-interacting models via the Hubbard-Stratonovich transformation.

The two approaches require the extrapolation of a discretization parameter, the logarithmic energy mesh parameter $\Lambda \rightarrow 1$ (NRG) and $\Delta\tau \rightarrow 0$ (HF-QMC), and have some limitations: The NRG effort grows exponentially with the number of localized AIM orbitals M , restricting the algorithm to $M \leq 2$, which prevents the usage of NRG for more realistic calculations where one would like to include, e.g., $M = 5$ or 7 orbitals for $3d$ and $4f$ systems, respectively. The HF-QMC on the other hand scales like $M^2(\beta/\Delta\tau)^3$ and, hence, quickly becomes too expensive in CPU time if temperature is decreased. This is a severe restriction since interesting many-body physics often occurs at low temperatures.

In this Letter, we introduce a new projective quantum Monte Carlo (PQMC) method for studying the zero-temperature AIM in the thermodynamic limit. Similar to projective approaches in lattice models [9], it relies on the idea that ground state properties are more efficiently obtained by filtering out – via projection along the imaginary time axis – the ground state wave function from a *suitably* chosen trial wave function. For the AIM, however, an efficient algorithm needs to be of the Hirsch-Fye type, in contrast to the lattice case [9]. In a second step, we incorporate this algorithm as an impurity solver within DMFT. In passing, we provide for a mandatory confirmation of the $T=0$ DMFT scenario for the Mott-Hubbard transition.

PQMC algorithm – Our starting point is the AIM Hamiltonian

$$H_{\text{AIM}} = H_0 + U n_{f\uparrow} n_{f\downarrow}, \quad (1)$$

$$H_0 = \sum_{\sigma} \epsilon_f n_{f\sigma} + \sum_{k\sigma} V_{k\sigma} (c_{k\sigma}^{\dagger} f_{\sigma} + \text{h.c.}) + \sum_{k\sigma} \epsilon_k c_{k\sigma}^{\dagger} c_{k\sigma}.$$

Here, f_{σ} (f_{σ}^{\dagger}) create (annihilate) impurity electrons with spin σ which interact via U and have a level energy ϵ_f ; $n_{f\sigma} = f_{\sigma}^{\dagger} f_{\sigma}$. These orbitals hybridize via $V_{k\sigma}$ with a conduction band (c_k^{\dagger}), having a dispersion ϵ_k .

Let us consider a trial wave function $|\Psi_T\rangle$ which is non-orthogonal to the (non-degenerate) ground state $|\Psi_0\rangle$ of the AIM. By means of the θ -projector $\sim \exp(-\theta H_{\text{AIM}}/2)$, we can filter out $|\Psi_0\rangle$ from $|\Psi_T\rangle$ and calculate ground state expectation values of an arbitrary operator \mathcal{O} :

$$\langle \mathcal{O} \rangle_0 = \frac{\langle \Psi_0 | \mathcal{O} | \Psi_0 \rangle}{\langle \Psi_0 | \Psi_0 \rangle} \quad (2)$$

$$= \lim_{\theta \rightarrow \infty} \frac{\langle \Psi_T | e^{-\theta H_{\text{AIM}}/2} \mathcal{O} e^{-\theta H_{\text{AIM}}/2} | \Psi_T \rangle}{\langle \Psi_T | e^{-\theta H_{\text{AIM}}} | \Psi_T \rangle}. \quad (3)$$

We now relate the projection formula to an artificial finite temperature ($1/\beta$) problem, using an auxiliary

Hamiltonian H_T whose ground state is $|\Psi_T\rangle$:

$$\langle \mathcal{O} \rangle_0 = \lim_{\theta \rightarrow \infty} \lim_{\tilde{\beta} \rightarrow \infty} \frac{\text{Tr} \left[e^{-\tilde{\beta} H_T} e^{-\theta H_{\text{AIM}}/2} \mathcal{O} e^{-\theta H_{\text{AIM}}/2} \right]}{\text{Tr} \left[e^{-\tilde{\beta} H_T} e^{-\theta H_{\text{AIM}}} \right]}. \quad (4)$$

With this trick, the r.h.s. of Eq. (4) is in a suitable form to apply (or rederive) the Hirsch-Fye algorithm at finite values of β . In the following, we will point out the necessary steps in short, more details will be published elsewhere [10].

We discretize imaginary time into Trotter slices of length $\Delta\tau$ and decouple the Coulomb interaction via the Hubbard-Stratonovich transformation. Let us now restrict to single-particle trial wave functions $|\Psi_T\rangle$ and Hamiltonians H_T . Then, the interaction (and the Hubbard-Stratonovich field) is zero for the $\tilde{\beta}$ part, and we can combine the propagation of this part ($\exp[-\tilde{\beta} H_T]$) with the H_0 part of the first θ Trotter slice ($\exp[-\Delta\tau H_0]$). The limit $\tilde{\beta} \rightarrow \infty$ can now be taken analytically, leaving a problem on the interval $[0, \theta]$ discretized into $L = \theta/\Delta\tau$ steps. As the HF-QMC, our PQMC algorithm deals with $L \times L$ matrices for the f-electron Green function on this interval. The updating equations for these Green functions (if a Hubbard-Stratonovich field is changed) are the same as that of HF-QMC. Choosing $H_T = H_0$, also the starting Green function (with all Hubbard-Stratonovich fields zero) has a similar structure: In HF-QMC it is the finite-temperature non-interacting Green function. In our PQMC algorithm it is – because of the extra $\tilde{\beta} \rightarrow \infty$ projection – the zero-temperature non-interacting Green function $\mathcal{G}_0(\tau, \tau')$ truncated to $0 \leq \tau, \tau' \leq \theta$. But with this different object (initial Green function), the same program code can actually be used.

Our PQMC algorithm allows the measurement of the Green function $G(\tau, \tau')$ but also of arbitrary correlation functions, θ -projected from the Slater determinant of the non-interacting AIM as a trial wave function $|\Psi_T\rangle$. For a meaningful PQMC calculation, we should measure all correlation functions only on the central \mathcal{L} time slices. Then $\mathcal{P} = (L - \mathcal{L})/2$ time slices on the right and left side of the measuring interval serve for projection. In the following, QMC results are understood in this sense.

DMFT self-consistency implementation – We now implement this algorithm as an impurity solver in the DMFT self-consistency cycle. Let us consider the half-filled Hubbard model

$$H = -t \sum_{\langle i, j \rangle \sigma} c_{i\sigma}^\dagger c_{j\sigma} + U \sum_i n_{i\uparrow} n_{i\downarrow}, \quad (5)$$

where $\langle i, j \rangle$ denotes the restriction to nearest neighbor hopping in d dimensions. We use the Bethe lattice with semicircular density states $N(E) = \frac{8}{\pi W^2} \sqrt{W^2/4 - E^2}$. In the following, units are normalized to a bandwidth $W = 4$.

DMFT [4] maps the Hubbard model onto an AIM with non-interacting Green function

$$\mathcal{G}_0(i\omega_n) = [G^{-1}(i\omega_n) + \Sigma(i\omega)]^{-1}, \quad (6)$$

where ω_n denote Matsubara frequencies. The Green function $G(i\omega_n)$ of the AIM has to be determined self-consistently together with the self energy $\Sigma(i\omega)$. Both are connected by the \mathbf{k} -integrated Dyson equation

$$G(i\omega_n) = \int dE \frac{N(E)}{i\omega - E - \Sigma(i\omega_n)}. \quad (7)$$

Thereby, the DMFT self-consistency cycle is as follows:

$$\Sigma(i\omega_n) \xrightarrow{(7)} G(i\omega_n) \xrightarrow{(6)} \mathcal{G}_0(i\omega_n) \xrightarrow{\text{PQMC}} G(\tau) \xrightarrow{(6)} \Sigma(i\omega_n) \dots$$

For the difficult task, i.e., calculating the zero temperature Green function $G(\tau)$ of the AIM for a given $\mathcal{G}_0(\tau)$ with $\tau \in [-\theta, \theta]$, we use the PQMC algorithm, instead of HF-QMC [11]. Since the PQMC Green function $G(\tau)$ is only defined for $\tau \leq \mathcal{L}\Delta\tau$, we first extrapolate $G(\tau)$ to large τ 's before Fourier transforming to Matsubara frequencies in the above self-consistency cycle. To this end, we employ the maximum entropy method, yielding the spectral function $A(\omega)$ which allows to calculate $G(i\omega_n) = \int d\omega \frac{A(\omega)}{i\omega_n - \omega}$ at any frequency $i\omega_n$. It is important to note that, in the end, this procedure only serves as a fit in imaginary time. Hence, we do not suffer from the usual problem – determining $A(\omega)$ from $G(\tau)$ is ill-conditioned. Only for very small $i\omega_n$, corresponding to the extrapolation in imaginary time, this procedure eventually breaks down.

Results – We will now use our PQMC method to study the interaction driven Mott-Hubbard metal-insulator transition that occurs at half filling. First, in Fig. 1 we illustrate the power of the PQMC method in direct comparison with finite- T HF-QMC results. We choose equal values of inverse temperature β and total projection time θ , having an identical number of Trotter time slices for both calculations. Then, our results for $\beta = \theta$ are obtained with a comparable numerical effort. For $U = 4.8$ and at low T , the DMFT equations have two solutions, where we follow the metallic solution (as soon as it exists). In the case of DMFT calculations with finite- T HF-QMC, the double occupancy per site $D = \langle n_\uparrow n_\downarrow \rangle$ of Fig. 1 starts at high temperatures ($\beta = 10$) in the insulating phase and only after the transition to the metallic phase around $\beta = 40$ convergence to the ground state value sets in. In contrast, the PQMC double occupancy convergences much faster and extrapolates almost linearly to the $T=0$ value. For example, the $\theta = 10$ PQMC result is even closer to the $T=0$ result than the HF-QMC double occupation at $\beta = 30$. Since the numerical effort grows cubically with θ or β this means that the PQMC is roughly 27-times faster at the same accuracy. We attribute this behavior to the absence of thermal fluctuations in PQMC.

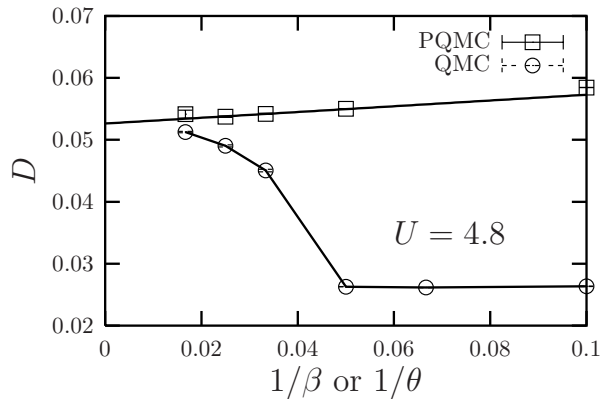


FIG. 1: DMFT double occupancy $D = \langle n_{\uparrow} n_{\downarrow} \rangle$ as a function of (i) temperature $T = 1/\beta$ (conventional HF-QMC; circles) and (ii) the inverse projection parameter $1/\theta$ (PQMC, squares). For $\theta = \beta$ the numerical effort is comparable, but the PQMC results converge much faster and almost linearly to the $T = 0$ value. Here and in the following, the bandwidth $W = 4$ sets the energy unit.

In the following, we present our results for the Mott-Hubbard metal-insulator transition, starting with the double occupation in Fig. 2. All calculations are done at a fixed $\Delta\tau = 0.2$. Upon increasing U , we systematically follow the metallic solution until at $U_{c2} \approx 6.0$ the metallic quasiparticle peak disappears. For the insulating solution on the other hand, we decrease the interaction until the insulator becomes unstable below $U_{c1} \approx 5.0$. Within the uncertainty of roughly 0.1-0.2, our coexistence region $U_{c1} < U < U_{c2}$ compares well with NRG results ($U_{c1} = 4.78$, $U_{c2} = 5.88$ [12, 13]). Already the $\beta = 20$ results (circles) for the double occupancy yield a good estimate for the low temperature coexistence region. In order to resolve the increasingly sharp quasiparticle peak in the vicinity of the critical point we also used longer projection times θ and the thick line represents a linear extrapolation for three values $\theta = 20, 30, 40$. Also plotted is the result from a 10th order perturbation expansion [14] in t/U , which agrees well with our results for the insulator. Our results are consistent with a linear dependence $(D_{\text{met}} - D_{\text{ins}}) \propto (U - U_{c2})$ which may be integrated to a groundstate energy $(E_{\text{met}} - E_{\text{ins}}) \propto (U - U_{c2})^2$ corresponding to a second order transition at U_{c2} [16].

Fig. 3 plots the local spin susceptibility $T\chi_{\text{loc}}(0) = \lim_{\theta \rightarrow \infty} \frac{1}{\theta} \int_0^{\theta} \langle S^z(\tau) S^z \rangle d\tau$, and actually represents the first DMFT analysis of this quantity through the zero temperature Mott-Hubbard metal-insulator transition (at finite- T it was studied in [15]). In the top panel, we observe the local moment behavior of the insulating solution without any sign of criticality at U_{c2} . On the other hand approaching U_{c2} from the metallic side, χ_{loc} is expected to diverge, reflecting the critical behavior of a Fermi liquid with a vanishing quasiparticle weight Z [16]. Therefore the second order character of the phase transition at U_{c2}

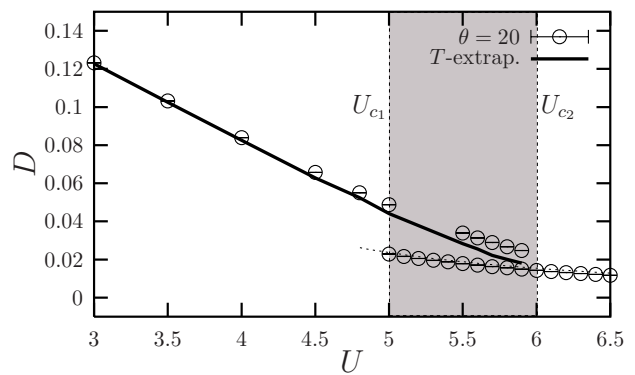


FIG. 2: Double occupancy $D = \langle n_{\uparrow} n_{\downarrow} \rangle$ as a function of interaction U for both metallic and insulating DMFT solutions. In the interval $5.0 \approx U_{c1} < U < U_{c2} \approx 6.0$ both solutions coexist (shaded region). Circles: $\theta = 20$; thick line: extrapolation to $\theta \rightarrow \infty$; dashed line: strong coupling expansion of [14].

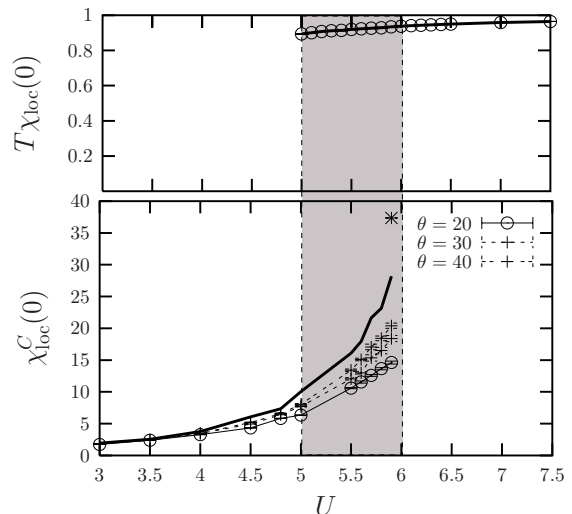


FIG. 3: Static local spin susceptibility $T\chi_{\text{loc}}(0)$ vs. U for the insulating (upper panel) and metallic DMFT solution (lower panel). For the metal, $\chi_{\text{loc}}(0)$ diverges as we approach U_{c2} from below. Since we plot the truncated integral χ_{loc}^C , the divergence is cut off at $\chi_{\text{loc}}^C = 37.4$ (star).

can only be observed for $U < U_{c2}$. For the metallic phase, we integrate the spin correlation function up to a maximal cutoff C : $\chi_{\text{loc}}^C(0) = \int_0^C \langle S^z(\tau) S^z \rangle d\tau$. The thick line is an extrapolation of χ_{loc}^C for a fixed cutoff $C = 40$ to $\theta \rightarrow \infty$, i.e., to the groundstate value. At the critical point, we see indications for a divergence of χ_{loc} which for the cutoff quantity χ_{loc}^C means approaching the star ($\chi_{\text{loc}}^C = 37.4$, the value of the insulating solution).

Finally, we present in Fig. 4 the spectra at $U = 5.9$, close to the phase transition. The insulating solution ($\theta = 20$) has a pronounced charge gap of around 1.2 between two Hubbard bands. The metallic solution shows an additional quasiparticle peak which is pinned to the non-interacting value, a consequence of Fermi liquid theory at $T = 0$ [17]. The quasiparticle peak for a fixed

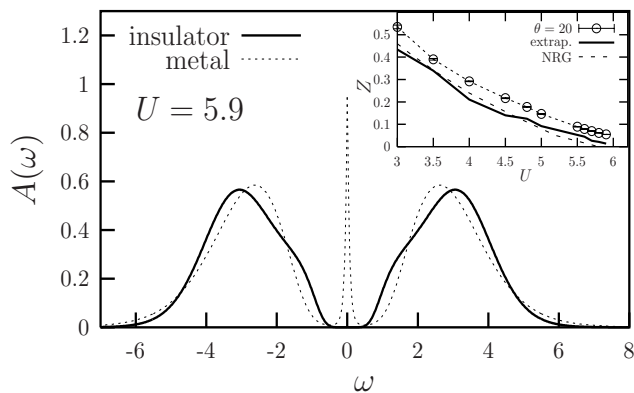


FIG. 4: Spectral functions $A(\omega)$ for the insulating (line) and metallic solution (dashed) close to the phase transition at $U = 5.9$. Inset: Quasiparticle weight Z vs. U for $\theta = 20$ (circles) and extrapolated to $\theta \rightarrow \infty$ (thick line), compared with NRG [12] (dashed line).

$\theta = 40$ has width of 0.05 (Note, that the low energy accuracy is limited by $1/\theta$ and the statistical quality of QMC data.). We determine the quasiparticle weight by $Z = \left(1 - \frac{\text{Im}\Sigma(i\omega_1)}{\omega_1}\right)^{-1}$ from the first Matsubara frequency. In principle, ω_1 can be chosen to be arbitrarily small, but controlled values for $\Sigma(i\omega_n)$ are restricted by the projection length $1/\theta$ and the maximum entropy extrapolation fit. The inset in Fig. 4 shows that at $\theta = 20$ the weight Z is still too large. But after extrapolating Z from $\theta = 20, 30, 40$ to $\theta \rightarrow \infty$, we find agreement with the NRG results [12].

Summary – We have introduced a novel projective (PQMC) algorithm for impurity models, which is on the technical front closely related to the standard Hirsch-Fye algorithm. The numerical effort for both algorithms is identical, but the convergence to the ground state is dramatically improved by PQMC. Using PQMC as an impurity solver for DMFT, we were able to obtain accurate zero temperature results for the Mott-Hubbard metal-insulator transition. There has been a strong controversy about the nature of this Mott-Hubbard transition within DMFT, in particular, whether two solutions (metallic and insulating) coexist in an interval $U_{c1} < U < U_{c2}$ or not. While the coexistence is by now generally accepted, NRG calculations [12] represent the only unsailable zero-temperature confirmation of the coexistence scenario [4]. Since other numerical results at $T = 0$ [18] and analytical arguments [19] contradict this scenario, an independent numerical study is certainly in order. Using PQMC, we have provided for such a mandatory reconfirmation, and beyond it we presented results for the double occupancy and local susceptibility.

Outlook – In recent years, there have been two main lines of DMFT developments: towards realistic calculations such as LDA+DMFT [20] and towards the inclu-

sion of more and more (non-local) correlations by means of cluster DMFT calculations [21]. These approaches require additional orbitals and DMFT sites, respectively, making NRG prohibitively CPU-expensive since the effort scales exponentially with more orbitals and sites. In contrast, our PQMC algorithm only scales quadratically or cubically, and hence opens the door to accessing low temperatures within realistic approaches or model-oriented calculations with non-local correlations.

We thank N. Blümer for discussions. This work was supported in part by the Deutsche Forschungsgemeinschaft through the Emmy Noether program.

-
- [1] D. Goldhaber-Gordon *et al.*, Nature **391**, 156 (1998); L. Kouwenhoven and L. Glazman, Physics world, January 2001, p. 33.
 - [2] V. Madhavan *et al.*, Science **280**, 567 (1998); J. Li *et al.*, Phys. Rev. Lett. **80**, 2893 (1998).
 - [3] W. Metzner and D. Vollhardt, Phys. Rev. Lett. **62**, 324 (1989); G. Kotliar and D. Vollhardt, Physics Today, March 2004, p. 53.
 - [4] A. Georges *et al.*, Rev. Mod. Phys. **68**, 13 (1996).
 - [5] N. Andrei, Phys. Rev. Lett. **45**, 379 (1980); P. B. Wiegmann, Sov. Phys. JETP Lett. **31**, 392 (1980); Phys. Lett. A **80**, 163 (1980); N. Kawakami and A. Okiji Phys. Lett. A **86**, 483 (1981).
 - [6] K. G. Wilson Rev. Mod. Phys. **47**, 773 (1975).
 - [7] J. E. Hirsch and R. M. Fye, Phys. Rev. Lett. **56**, 2521 (1986).
 - [8] P.W. Anderson, J. Phys. C **3**, 2436 (1970).
 - [9] G. Sugiyama and S.E. Koonin, Annals of Phys. **168**, 1 (1986); S. Sorella, S. Baroni, R. Car, and M. Parrinello, Europhys. Lett. **8**, 663, (1989); M. Imada and Y. Hatsugai, J. Phys. Soc. Jpn. **58**, 3752 (1989).
 - [10] M. Feldbacher, K. Held, and F. F. Assaad, in preparation.
 - [11] M. Jarrell, Phys. Rev. Lett. **69**, 168 (1992).
 - [12] R. Bulla, Phys. Rev. Lett. **83**, 136 (1999).
 - [13] R. Bulla, T. A. Costi, and D. Vollhardt, Phys. Rev. B **64**, 45103 (2001).
 - [14] N. Blümer and E. Kalinowski, cond-mat/0404568.
 - [15] M. J. Rozenberg, G. Kotliar, and X. Y. Zhang, Phys. Rev. B **55**, 2082 (1997).
 - [16] G. Moeller *et al.*, Phys. Rev. Lett. **74**, 2082 (1995).
 - [17] E. Müller-Hartmann, Z. Phys. B **76**, 211 (1989).
 - [18] R. Noack and F. Gebhard, Phys. Rev. Lett. **82**, 1915 (1999).
 - [19] P. Nozières, Eur. Phys. J. B **6**, 447 (1998); D. E. Logan and P. Nozières, Philos. Trans. R. Soc. London A **356**, 249 (1998); S. Kehrein Phys. Rev. Lett. **81**, 3192 (1998).
 - [20] V.I. Anisimov *et al.*, J. Phys. Cond. Matter **9**, 7359 (1997); K. Held *et al.*, Psi-k Newsletter #56 (2003), p. 5 [psi-k.dl.ac.uk/newsletters/News_56/Highlight_56.pdf]; A. I. Lichtenstein, M. I. Katsnelson, and G. Kotliar, to be published in *Electron Correlations and Materials Properties 2*, ed. A. Gonis (Kluwer, NY).
 - [21] Th. Maier *et al.*, cond-mat/0404055.